Materials Advances

ROYAL SOCIETY OF CHEMISTRY

PAPER

View Article Online
View Journal | View Issue

Cite this: *Mater. Adv.*, 2022, 3, 9083

Enabling water-free PEDOT as hole selective layer in lead-free tin perovskite solar cells†

Diego Di Girolamo, ‡[a] Ece Aktas, ‡[a] Corinna Ponti, ‡[a] Jorge Pascual, [b] Guixiang Li, [c] Meng Li,[c] Giuseppe Nasti,[a] Fahad Alharthi, [d] Francesco Mura[e] and Antonio Abate*[acd]

Received 19th July 2022,
Accepted 11th October 2022

DOI: 10.1039/d2ma00834c

rsc.li/materials-advances

Metal halide perovskites are set to revolutionise photovoltaic energy harvesting owing to an unmatched combination of high efficiency and low fabrication costs. However, to improve the sustainability of this technology, replacing lead with less toxic tin is highly desired. Tin halide perovskites are approaching 15% in power conversion efficiency (PCE), mainly employing PEDOT:PSS as a hole-selective layer. Unfortunately, PEDOT:PSS is processed from an aqueous solution, which is hardly compatible with the strict anoxic requirements for processing tin halide perovskites due to tin's instability to oxidation. Here, we present a water-free PEDOT formulation for developing tin-based lead-free perovskite solar cells. We show that the main difference between the PCE of devices made from aqueous and water-free PEDOT is due to the marked hydrophobicity of the latter, which complicates the perovskite deposition. By modifying the surface of water-free PEDOT with a thin Al_2O_3 interlayer, we could achieve good perovskite morphology that enabled perovskite solar cells with a PCE of 7.5%.

Introduction

Halide perovskite photovoltaics (PV) are the frontrunner technology to revolutionise the role of PV in energy production for the next decades.[1] The high performance, along with an unprecedented versatility regarding the processing and the properties of the material make halide perovskite PV a strong candidate for all possible futuristic PV applications: from high-efficiency tandem solar cells with silicon PV[2] to building-integrated photovoltaics (BIPV)[3] or even flexible, stretchable and wearable PV.[4] It is essential to consider the stability limit of perovskite PV,[5] which poses concerns over its application for power generation units in the kW (microgrid and residential) – MW (commercial, industrial, and utility) scale or for BIPV, which is much less critical for application in IoT or consumer electronics, where the lifetime required is lower than 30 years. Hence, the sustainability of the technology is a matter of debate, especially considering the end-of-life of perovskite solar cells. In addition, the presence of lead in the crystalline structure of the perovskite itself is a severe problem which deserves all the efforts of the R&D community to be tackled. Lead is among the ten most toxic species as listed by World Health Organization (WHO),[6] mainly due to its calcium-mimicking activity in the human metabolism and its enhanced negative effect on the brain development of infants. The main approaches to tackle this lead issue are introducing lead-sequestering layers into the device design[7] and developing lead-free perovskite compositions.[8,9] The latter would be a much more resolutive solution, and tin has been identified as the most promising alternative to lead. Tin and lead are in the same group of the periodic table and share many similar physicochemical properties. For instance, the ionic radius and the presence of an ns^2 lone pair in the +2-oxidation state are crucial in defining the crystal structure and optoelectronic properties of the halide perovskites. Mixed-tin and lead-free perovskite solar cells surpassed 23%[10] and 14% PCE.[11] The main difference between tin and lead is the higher relative instability of the +4-oxidation state for tin, which is oxidised by air or even by mildly oxidising solvents.[12,13] This fact has a tremendous impact on the defect chemistry of tin perovskites and renders extremely more challenging the synthesis of high-quality tin halide perovskites.

In our previous work, we tackled the oxidation of tin from dimethyl sulfoxide (DMSO) by proposing a set of alternative

[a] *Department of Chemical, Materials and Production Engineering, University of Naples Federico II, Piazzale Tecchio 80, Fuorigrotta 80125, Italy. E-mail: antonio.abate@unina.it*
[b] *Institute for Chemical Research, Kyoto University, Gokasho, Uji, Kyoto 611-0011, Japan*
[c] *Helmholtz-Zentrum Berlin für Materialien und Energie GmbH, Berlin 14109, Germany*
[d] *Chemistry Department, Science College, King Saud University, P O Box 2455, Riyadh 11451, Saudi Arabia*
[e] *Centro delle Nanotecnologie applicate all'Ingegneria della Sapienza – CNIS, University of Rome La Sapienza, Piazzale Aldo Moro 5, Rome 00185, Italy*

† Electronic supplementary information (ESI) available. See DOI: https://doi.org/10.1039/d2ma00834c

‡ Contributed equally to this work.

solvents.[14] Here, we focus on another part of the device which poses concerns regarding its compatibility with tin perovskite, the hole selective layer (HSL).

To date, all the most efficient tin halide perovskite solar cells comprise PEDOT:PSS as a hole selective layer.[8,11] This fact may seem counterintuitive since this material has been soon discarded from lead perovskite solar cells due to its poor interface properties and stability issues. The fundamental reason behind the success of PEDOT:PSS in tin perovskites is still unknown. A hypothesis is that its shallower valence band compared to alternative HSLs favours a better energy alignment with the tin perovskites valence band. Nonetheless, the fact that PEDOT:PSS is processed from an aqueous solution could be a problem in future large-scale production, for instance in roll-to-roll or sheet-to-sheet production lines, where the presence of water is not compatible with the strong anoxic requirements for the production of tin perovskites.

The development of water-free PEDOT formulations is a topic of industrial interest, and some alternatives are commercially available. Moreover, the adoption of water-free PEDOT contacts has been demonstrated feasible in lead halide perovskite solar cells, with a positive effect on the stability of devices.[15] This work demonstrates the possibility of adopting a water-free PEDOT formulation in lead-free tin perovskite solar cells. We show how to tune the surface energy of the water-free PEDOT to allow the formation of a high-quality perovskite film over macroscopic areas. We show a careful perovskite optimisation to achieve a PCE of 7.5% for DMSO-free tin perovskite solar cells.

Results

The most evident difference when moving from standard aqueous PEDOT:PSS to water-free PEDOT composition is the change of the surface polarity from hydrophilic to hydrophobic. This fact strongly impacts the substrate properties of the PEDOT layer for perovskite growth. From a practical standpoint, the perovskite solution has difficulty spreading over the whole substrate during spin-coating (exacerbated in dynamical dispensing). Nonetheless, good coverage can be reproducibly achieved with some care in distributing the solution before starting the spin ramp. However, in this case, we also observed an inferior morphology at the nanoscale. In Fig. 1a, we show the scanning electron microscopy (SEM) top view micrograph of the $FASnI_3$ (FA: formamidinium) film deposited from *N*,*N*-diethylformamide:*N*,*N*′-dimethylpropyleneurea (DEF:DMPU) with toluene as antisolvent, as we optimised on aqueous PEDOT:PSS in our previous work.[14] The grains were tiny (<100 nm) with a poorly defined shape, pointing to a poor crystallinity of the material. Moreover, small pinholes were present with micron-scale spacing among them. By enlarging the view, we could also observe aggregates with poor electrical contact with the substrates (the strong white colour is attributed to electron accumulation during the SEM measurement). This is substantially different from what we achieved on

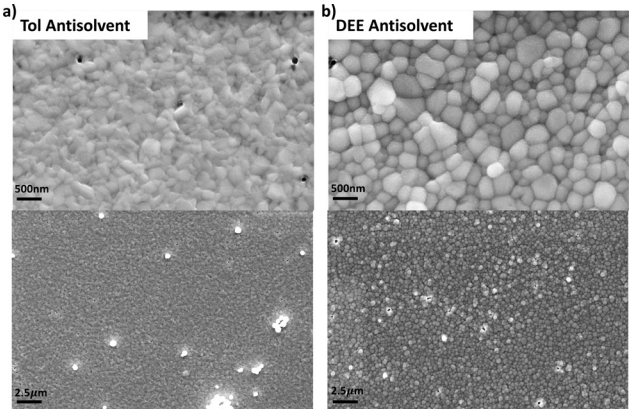

Fig. 1 The role of antisolvent on $FASnI_3$ morphology. Top-view SEM micrographs at 50k (top) and 10k (down) magnification of $FASnI_3$ thin films deposited on water-free PEDOT formulation by employing (a) toluene (Tol) and (b) DEE as antisolvent.

aqueous PEDOT, where a typical perovskite morphology with 200–300 nm diameter spherical grains was obtained. Interestingly, the quality of the perovskite film could be tuned by selecting a different antisolvent. We got an excellent perovskite morphology by employing diethyl ether (DEE), as shown in Fig. 1b. Unfortunately, in this case, by enlarging the view, we could observe the appearance of pinholes with a 1–10 micron-scale spacing and few aggregates, showing some criticalities yet to be solved.

When looking at the film on the cm scale, the one processed from DEE on water-free PEDOT presented many macroscopic pinholes, as shown in the back-illuminated picture in Fig. 2a. We anticipated that the presence of such pinholes in many cases would lead to not working devices. In our experience, the presence of macroscopic pinholes in the perovskite films is usually observed when depositing the perovskite on poorly wetting substrates, such as poly[bis(4-phenyl)(2,5,6-trimethylphenyl)amine (PTAA).[16] Thus, we introduced a thin Al_2O_3 nanoparticles interlayer to modify the wettability of the water-free PEDOT, as shown for other polymeric hole selective layers.[17] Despite being an insulator, Al_2O_3 has found application in perovskite PV as an interlayer;[18] nonetheless, we aimed at introducing the smallest amount to modify the wetting properties of PEDOT while not raising eventual barriers to charge transport. By spin-coating a 1 : 50 (vol : vol) diluted Al_2O_3 dispersion in an ethanol solution, we substantially improved the wettability of the water-free PEDOT for the perovskite solution. In Fig. 2, we characterised the variation of the contact angle of the perovskite solution deposited on top of different substrates. Noteworthy, when moving from aqueous (Fig. 2c) to water-free PEDOT (Fig. 2d), the contact angle increased from 32.6° (excellent wettability) to 106° (low wettability). The introduction of a thin Al_2O_3 (contact angle of 17.5° *per se*) on top of the water-free PEDOT reduced the contact angle down to 61.8° (decent wettability), allowing easy processing of the perovskite film (Fig. 2e and f). Confirming our hypothesis, the improvement of the wettability upon Al_2O_3

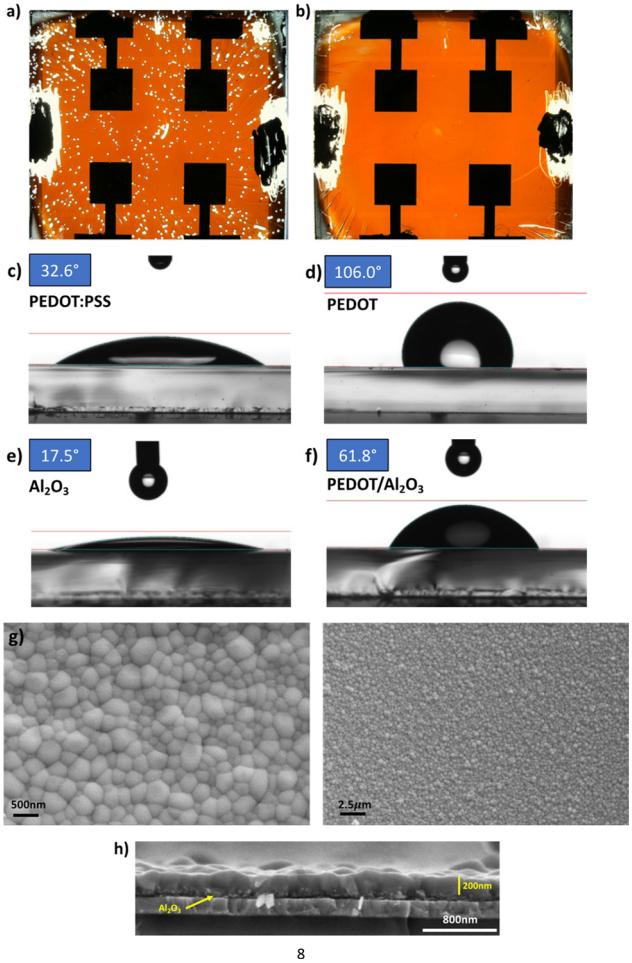

Fig. 2 The role of Al_2O_3 in the improvement of large-area uniformity of perovskite films. Retro-illuminated photographs of a substrate comprising four different ~0.17 cm^2 area $FASnI_3$ solar cells adopting (a) water-free PEDOT and (b) water-free PEDOT/Al_2O_3 as the substrate for perovskite growth. Contact angle measurements of a perovskite solution drop on (c) PEDOT:PSS (d) water-free PEDOT (e) Al_2O_3 nanoparticles film and (f) water-free PEDOT with thin Al_2O_3 nanoparticles film substrates. (g) Top-view SEM micrographs at 50k (left) and 10k (right) magnification of $FASnI_3$ thin film deposited on water-free PEDOT/Al_2O_3 employing DEE as antisolvent. (h) Cross-sectional SEM micrograph of the glass/ITO/water-free PEDOT/Al_2O_3/$FASnI_3$ stack.

introduction allowed easier processing of the perovskite film on top of the water-free PEDOT. It ultimately resulted in the complete removal of the microscopic pinholes, as shown in Fig. 2b.

Notably, the Al_2O_3 interface modification enormously improved the nanoscale appearance of the perovskite films, showing a good morphology over a micron-scale with no pinholes or aggregates from the SEM top view of the $FASnI_3$ film deposited on the PEDOT/Al_2O_3 substrate, as we show in Fig. 2g. The cross-section of the stack highlights a thickness of around 200 nm for the perovskite layer, and no voids at the PEDOT/perovskite interface with the Al_2O_3 interlayer can be observed as thin (<50 nm) and discontinuous (Fig. 2h).

The interfacing of metal oxides and halide perovskites is a well-known source of degradation. Metal oxides trigger chemical reactions involving halides or amines, including acid-base or redox chemistry.[19–21] In the case of tin perovskites, the instability towards metal oxides could be exacerbated by the possibility of oxidising Sn^{2+}. Zhidkov *et al.* reported the oxidation of Sn following thermal degradation of ITO/$MASnI_3$ stacks (where ITO is indium tin oxide).[22] More recently, Chen *et al.* reported evidence of severe oxidation of $FASnI_3$ when in contact with NiO.[23] To verify the suitability of Al_2O_3 as a contact material for tin halide perovskites, we conducted a thermal stress experiment of $FASnI_3$/metal oxide powder mixtures characterised by photoluminescence (PL) spectroscopy. We opted for NiO as the control material, following the work of Chen. Interestingly, the interfacing of $FASnI_3$ and NiO powders resulted in an increasing blueshift of the PL, which also broadened the emission feature upon prolonged thermal stress, as shown in Fig. 3a. As repeatedly reported, the blue shift of PL is a strong indication of oxidation of tin perovskites (with the Burstein-Moss effect due to doping or lattice distortion being the central hypothesis).[24–26] Thus, our observation confirms the oxidative degradation of $FASnI_3$ in contact with NiO. We did not observe any PL blueshift when we conducted the same experiment on $FASnI_3$/Al_2O_3 powder mixtures. For clarity, a slight decrease in the PL intensity was observed (see the background variation in Fig. 3b), suggesting that the thermal stress introduces defects into the perovskite powders but not through an oxidative mechanism. The difference between Al_2O_3 and NiO could be rationalised by invoking the different defect chemistries of the two metal oxides: NiO p-type conductivity arises from oxidising Ni^{3+} states compensating V''_{Ni}.[27] At the same time, Al_2O_3 cannot accommodate oxidation states different from Al^{3+} and O^{2-}. To a similar conclusion arrived Baranwal *et al.* measuring the conductivity of tin perovskite thin films growth on top of other metal oxides and attributing to Al_2O_3 the least oxidising activity.[28]

The control over the morphology of the perovskite films has been the most critical strategy for improving the PCE of perovskite PV.[29] Based on the films studied in this work, we expected to observe a strong correlation between the solar cells' morphology and PV performances. In Fig. 4a; "Tol" (black curve) identifies the perovskite layer processed with toluene as antisolvent (morphology in Fig. 1a), "DEE" (red curve) identifies the perovskite layer processed with DEE as antisolvent (morphology in Fig. 1b), "Al_2O_3" (blue curve) identifies the perovskite layer processed with DEE as antisolvent and Al_2O_3 as interlayer (morphology in Fig. 2g). The solar cells with $FASnI_3$ processed with toluene as antisolvent barely showed PV activity with a short-circuit current (J_{SC}) of 9.9 mA cm^{-2}. The open-circuit voltage (V_{OC}) was extremely low (126 mV) and the current-voltage (J–V) curve was a straight line. This result can be explained by the significant presence of pinholes at the nanoscale, strongly reducing the shunt resistance. Interestingly, the solar cells processed by DEE without Al_2O_3 were much more efficient, with a J_{SC} of 16.2 mA cm^{-2}, a V_{OC} of 348 mV and an FF of 62%. Removing the macroscopic pinholes (shown in Fig. 2a) with the Al_2O_3 interlayer further improved the device performance, with a J_{SC} of 17.2 mA cm^{-2}, a V_{OC} of

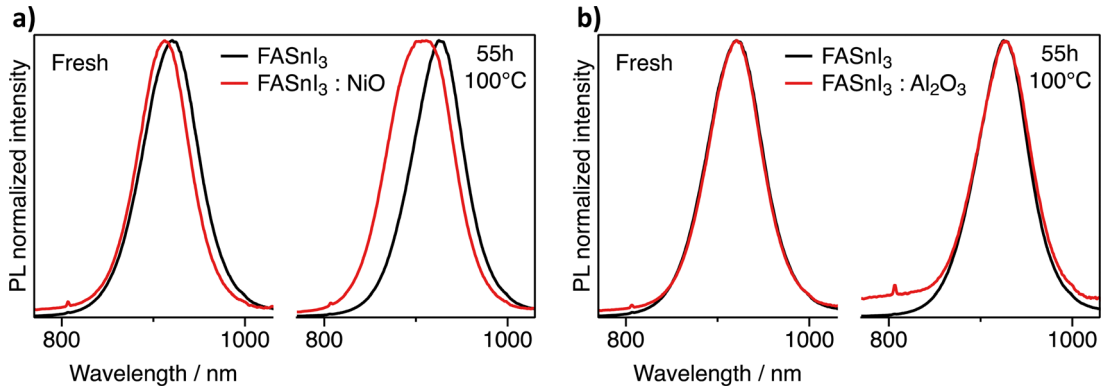

Fig. 3 Stability of Al_2O_3/$FASnI_3$ interface. (a) PL evolution of a $FASnI_3$/NiO powders mixture as prepared and after heating for 55 hours at 100 °C. It is possible to observe a blue shift of the PL, as usually observed when tin perovskites undergo oxidation. (b) PL evolution of a $FASnI_3$/Al_2O_3 powders mixture as prepared and after heating for 55 hours at 100 °C. In this case, the PL peak remains stable.

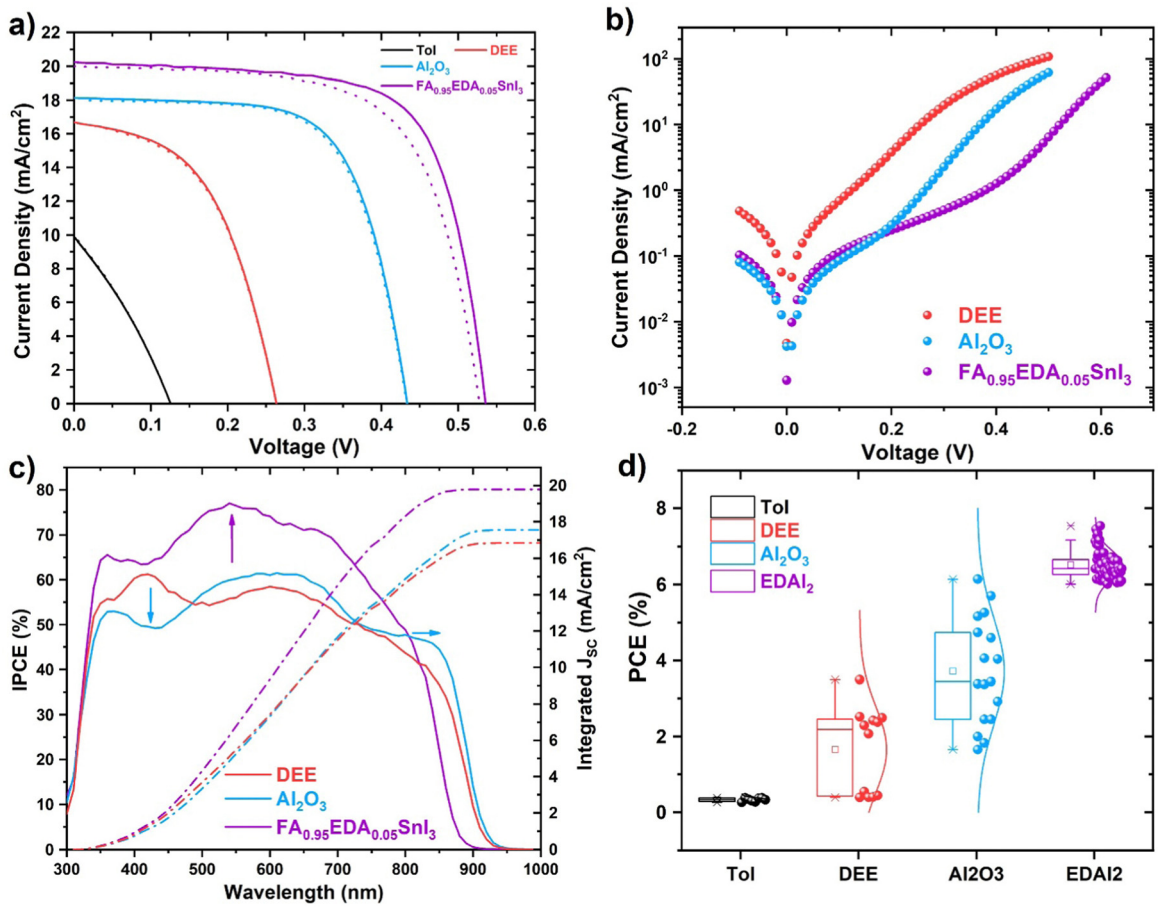

Fig. 4 Enabling $FASnI_3$ solar cells by antisolvent selection and Al_2O_3 interlayer and $EDAI_2$ improves reproducibility and performance. (a) The best *J*–*V* curves under simulated AM 1.5 G measured for $FASnI_3$-based solar cells with Tol, DEE, Al_2O_3 and $EDAI_2$ conditions. Both forward (solid lines) and reverse (dot lines) measurements are indicated. (b) Dark *J*–*V* curves for DEE, Al_2O_3 and $EDAI_2$ solar cells, showing a substantial reduction in the leakage current (the current density at 0 V). (c) IPCE and Integrated J_{SC} for DEE, Al_2O_3 and $EDAI_2$ solar cells. (d) Statistical distribution of PCE for the different devices discussed in this work.

443 mV and a fill factor (FF) of 67%, with a PCE above 5% (Table 1). By analysing the dark *J*–*V* curves for the devices with and without the Al_2O_3 interlayer, we confirmed that removing the pinholes increased the shunt resistance by at least one order of magnitude. In Fig. 4b, the leakage current for the Al_2O_3 device was one order of magnitude lower. The incident

Table 1 The PV parameters of the champion devices based on different conditions

Conditions	Integrated J_{SC} (mA cm^{-2})	J_{SC} (mA cm^{-2})	V_{OC} (mV)	FF (%)	PCE (%)
Tol	—	9.9	126	30	0.4
DEE	16.9	16.2	348	62	3.5
Al_2O_3	17.5	17.5	443	67	5.3
$EDAI_2$	19.8	20.2	535	69	7.5

photon-to-electron conversion efficiency (IPCE) shows that the introduction of the Al_2O_3 interlayer changed the spectral response of the device, worsening in the UV and blue region (below 500 nm) but improving it at larger wavelengths (Fig. 4c). In Fig. S3 (ESI†) we report the energy diagram for the devices with Al_2O_3. Due to its insulating nature Al_2O_3 should hinder the charge extraction, but the FF approaching 70% shows that this is not the case. Our observation is in line with previous reports where insulating materials, including metal oxides (Al_2O_3[30] or MgO[31]) or polymers (*e.g.* PMMA[32]) are introduced between the perovskite and the selective contacts to passivate the defects, improve the morphology or enhance the stability. Depending on the thickness and structure of such insulating layers the charge is expected to be extracted *via* tunnelling or pinholes. In our case, the Al_2O_3 layer is a nanoparticles film, and the charge reasonably flows through the pinholes.

An efficiency above 5% for an undoped $FASnI_3$ perovskite solar cell is close to the state of the art for the field. However, years of extensive efforts towards additive engineering enabled a PCE of over 14% for tin perovskite solar cells, even from the oxidising DMSO solvent. Unfortunately, as our previous work[33] discussed, the doping strategies developed from DMSO-based perovskite precursor solutions might not apply to our case. For instance, when introducing SnF_2,[34,35] we obtained material with no detectable light emission.[33] Interestingly, the successful doping strategy we could transfer from the standard DMSO-based processing is the introduction of ethylenediammonium diiodide ($EDAI_2$) into the perovskite composition.[36–38] Similarly to what was observed by Jokar *et al.*,[36] we could keep a progressive enlargement of the perovskite bandgap upon introducing $EDAI_2$, as visible from the blueshift of the PL peak maximum from 885 to 824 nm (see Fig. S1, ESI†). Solar cells, including $EDAI_2$-doped $FASnI_3$ perovskite on a water-free PEDOT/Al_2O_3 stack, showed improved efficiency and reproducibility. According to the literature, the positive effect of $EDAI_2$ is to enable the fabrication of pinhole-free tin perovskites and to passivate the surface. The latter could be the dominant mechanism in our case since we can obtain pinhole-free perovskite films without $EDAI_2$. Moreover, a careful analysis of the dark *J–V* current (Fig. 4b) shows a similar leakage current for devices with and without $EDAI_2$. The main difference is the lower dark current for devices with $EDAI_2$ at a voltage larger than 0.2 V, pointing to reduced recombination. In Fig. 4a, we plotted the *J–V* curve for the best-performing device, showing a J_{SC} of 19.8 mA cm^{-2}, a V_{OC} of 553 mV, a FF of 69% and negligible hysteresis at a 250 mV s^{-1} scan rate for a PCE of 7.53% (Table 1). The IPCE in Fig. 4b matched the J_{SC} obtained under the sun simulator and showed an IPCE approaching 80% in the green part of the solar spectrum (around 550 nm), overperforming the devices without $EDAI_2$. Besides the enhanced performances, the reproducibility was greatly improved, as shown in Fig. 4d. The devices based on pristine $FASnI_3$ showed a broad PCE distribution between 2 and 6%, similar to what we obtained on aqueous PEDOT.[14] On the other hand, $EDAI_2$-containing devices showed a narrower distribution, especially in V_{OC} and FF, resulting in a reproducible PCE between 6 and 8% (see Fig. S2, ESI†). In Fig. S4 (ESI†) we show the stable maximum power point tracking of the water-free PEDOT-based devices within a few minutes along with a slight increase in PCE in the first days of storing $EDAI_2$-containing devices.

Conclusions

In this work, we demonstrated a straightforward strategy to bridge the gap in the performances of lead-free tin perovskite solar cells between the standard aqueous PEDOT:PSS hole selective layer and water-free PEDOT formulations. The latter is desirable due to the better compatibility with the strict anoxic conditions required for processing tin perovskites. A good morphology of the perovskite film could be obtained by using diethyl ether as an antisolvent in place of toluene. Tuning the wettability of the perovskite solution on the water-free PEDOT by introducing a thin interlayer based on Al_2O_3 nanoparticles enabled the formation of a pinhole-free film and boosted the PCE above 5%. To further enhance the PCE of the devices, we introduced $EDAI_2$ as a dopant, obtaining a PCE of 7.5% and a narrow statistical distribution of the PV parameters.

These results prove that, despite the complicated fabrication of tin halide perovskites, solution wetting can be tuned accordingly to process high-quality thin films in DMSO-free conditions on more stable charge transporting materials. This work provides valuable guidelines for processing tin halide perovskites on new solutions and substrates with reduced content of oxidant species.

Experimental

Chemicals and materials

Formamidinium iodide was purchased from Dyenamo. We purchased water-free PEDOT-complex dispersion in toluene (HTL3) from Clevios™. All the other chemicals were purchased from Sigma Aldrich and used as received.

Solar cell fabrication

2.5 × 2.5 cm^2 pre-patterned ITO substrates (Kintec, 10 Ohm per square) were cleaned by subsequent sonication in Hellmanex 2% deionised water solution, water, acetone, and ethanol for 15 minutes at 40 °C. The well-dried ITO substrates were transferred to N_2 filled glovebox for plasma treatment. It is worth mentioning that the rest of the device fabrication was

carried out in a highly pure N_2-filled glovebox. Moreover, the glovebox atmosphere has never been contaminated by DMSO. The transferred ITO substrates were then plasma-treated for 15 minutes with an Electronic Diener plasma cleaner with an N_2 plasma at 0.3 mbar pressure. As hole selective contact, the diluted HTL3 solution spun at 4000 rpm for 25 seconds and annealed at 150 °C for 10 minutes. To improve wettability, diluted Al_2O_3 nanoparticles dispersion was spun at 4000 rpm for 25 seconds and annealed at 100 °C for 3 minutes. The $FASnI_3$ solution (1.2 M in 6 : 1 DEF : DMPU, with 10% over-stoichiometry of SnI_2 and eventually 5% $EDAI_2$) was spun at 500 rpm for 5 seconds and 4000 rpm for 25 seconds. After 21 seconds, 100 μL of DEE were dropped on the spinning substrate to induce the perovskite crystallisation. The film was annealed at 100 °C for 30 minutes. As electron selective contact, C_{60} (23 nm) and BCP (7 nm) were subsequently evaporated at a 10^{-6} mbar vacuum level with a deposition rate between 0.1 and 0.3 Å s^{-1}. Following, silver was evaporated through a shadow mask at a rate of 0.1 Å s^{-1} up to 2.5 nm, increasing to 0.3 Å s^{-1} up to 10 nm and then at 1 Å s^{-1} up to 100 nm. The completed device area is around 0.17 cm^2. The silver paste was applied to the contacts. The devices were stored overnight in a glovebox before measuring.

Solar cells and materials characterisation in glove box

The multimodal Arkeo machine has carried out the characterisation in glovebox from Cicci Research s.r.l. *J–V* curves were measured with a commercial apparatus (Arkeo-Ariadne, Cicci Research s.r.l.) based on a ring of 12LEDs ranging from 300 to 1000 nm and calibrated to fit class A and a 4-wire source meter. The IPCE spectrum was measured with a commercial apparatus (Arkeo-Ariadne, Cicci Research s.r.l.) based on a 300 Watt xenon lamp, able to acquire a spectrum from 300 to 1100 nm.

PL test is performed with a commercial platform (ARKEO-Cicci Research): the substrate is illuminated with a diode-pumped solid-state (DPSS) Nd:YVO4 + KTP Laser (Peak wavelength 532 nm ± 1 nm, optical power 1 mW on a circular spot of 2 mm of diameter: 31 mW cm^{-2}) at an inclination of 45°. The fluorescence on the same side of the substrate is focused on a bundle of fibres (10 mm in diameter) with an aspheric lens close to the substrate to maximise the PL. The bundle sends the signal to a CCD-based spectrometer. Integration time and the number of averaging is maintained the same to compare the results better.

The water contact angle measurements were performed with a Kruss Drop Shape Analysis System DSA25 outside the glovebox. The droplet volume was between 1 and 2 μL.

Author contributions

DDG conceived the idea of this study and wrote the first draft of the manuscript under the supervision of AA. DDG, EA and CP fabricated and characterised devices under the supervision of AA. EA carried out contact angle measurements. JP carried out PL measurements. FM, GL carried out SEM measurements under the supervision of ML. All authors participated in the discussion of the results and the manuscript writing and, finally, approved the submission.

Conflicts of interest

There are no conflicts to declare.

Acknowledgements

This work has received funding from the European Research Council (ERC) under the European Union's Horizon 2020 research and innovation programme (Grant agreement No. 804519). Authors thanks the Distinguished Scientist Fellowship Program (DSFP) at KSU for financial support. EA and AA acknowledge the European Union's Horizon 2020 research and innovation programme under the Marie Skłodowska-Curie grant agreement No 956270.

References

1 H. J. Snaith, *J. Phys. Chem. Lett.*, 2013, **4**, 3623–3630.
2 M. Jost, E. Kohnen, B. M.-V. Anna, L. Benjamin, J. Klaus, B. Macco, A. Al-ashouri, K. Janez, L. Korte, R. Bernd, S. Rutger, T. Marko, S. Bernd and A. Steve, *Energy Environ. Sci.*, 2018, 3511–3523.
3 M. Batmunkh, Y. L. Zhong and H. Zhao, *Adv. Mater.*, 2020, **32**, 2000631.
4 Y. Hu, T. Niu, Y. Liu, Y. Zhou, Y. Xia, C. Ran, Z. Wu, L. Song, P. Müller-Buschbaum, Y. Chen and W. Huang, *ACS Energy Lett.*, 2021, **6**, 2917–2943.
5 M. V. Khenkin, E. A. Katz, A. Abate, G. Bardizza, J. J. Berry, C. Brabec, F. Brunetti, V. Bulović, Q. Burlingame, A. Di Carlo, R. Cheacharoen, Y. B. Cheng, A. Colsmann, S. Cros, K. Domanski, M. Dusza, C. J. Fell, S. R. Forrest, Y. Galagan, D. Di Girolamo, M. Grätzel, A. Hagfeldt, E. von Hauff, H. Hoppe, J. Kettle, H. Köbler, M. S. Leite, S. (Frank) Liu, Y. L. Loo, J. M. Luther, C. Q. Ma, M. Madsen, M. Manceau, M. Matheron, M. McGehee, R. Meitzner, M. K. Nazeeruddin, A. F. Nogueira, Ç. Odabaşı, A. Osherov, N. G. Park, M. O. Reese, F. De Rossi, M. Saliba, U. S. Schubert, H. J. Snaith, S. D. Stranks, W. Tress, P. A. Troshin, V. Turkovic, S. Veenstra, I. Visoly-Fisher, A. Walsh, T. Watson, H. Xie, R. Yıldırım, S. M. Zakeeruddin, K. Zhu and M. Lira-Cantu, *Nat. Energy*, 2020, **5**, 35–49.
6 WHO, *World Heal. Organ.*, 2019, 1–6.
7 X. Li, F. Zhang, H. He, J. J. Berry, K. Zhu and T. Xu, *Nature*, 2020, **578**, 555–558.
8 K. Nishimura, M. A. Kamarudin, D. Hirotani, K. Hamada, Q. Shen, S. Iikubo, T. Minemoto, K. Yoshino and S. Hayase, *Nano Energy*, 2020, **74**, 104858.
9 T. Wu, X. Liu, X. Luo, X. Lin, D. Cui, Y. Wang, H. Segawa, Y. Zhang and L. Han, *Joule*, 2021, **5**, 863–886.
10 S. Hu, K. Otsuka, R. Murdey, T. Nakamura, M. A. Truong, T. Yamada, T. Handa, K. Matsuda, K. Nakano, A. Sato,

K. Marumoto, K. Tajima, Y. Kanemitsu and A. Wakamiya, *Energy Environ. Sci.*, 2022, **15**, 2096–2107.
11 X. Jiang, H. Li, Q. Zhou, Q. Wei, M. Wei, L. Jiang, Z. Wang, Z. Peng, F. Wang, Z. Zang, K. Xu, Y. Hou, S. Teale, W. Zhou, R. Si, X. Gao, E. H. Sargent and Z. Ning, *J. Am. Chem. Soc.*, 2021, **143**, 10970–10976.
12 M. I. Saidaminov, I. Spanopoulos, J. Abed, W. Ke, J. Wicks, M. G. Kanatzidis and E. H. Sargent, *ACS Energy Lett.*, 2020, **5**, 1153–1155.
13 J. Pascual, G. Nasti, M. H. Aldamasy, J. A. Smith, M. Flatken, N. Phung, D. Di Girolamo, S.-H. Turren-Cruz, M. Li, A. Dallmann, R. Avolio and A. Abate, *Mater. Adv.*, 2020, **1**, 1066–1070.
14 D. Di Girolamo, J. Pascual, M. H. Aldamasy, Z. Iqbal, G. Li, E. Radicchi, M. Li, S. H. Turren-Cruz, G. Nasti, A. Dallmann, F. De Angelis and A. Abate, *ACS Energy Lett.*, 2021, 959–968.
15 L. Kegelmann, P. Tockhorn, C. M. Wolff, J. A. Márquez, S. Caicedo-Dávila, L. Korte, T. Unold, W. Lövenich, D. Neher, B. Rech and S. Albrecht, *ACS Appl. Mater. Interfaces*, 2019, **11**, 9172–9181.
16 Z. Bagheri, F. Matteocci, E. Lamanna, D. Di Girolamo, A. G. Marrani, R. Zanoni, A. Di Carlo and A. Moshaii, *Sol. Energy Mater. Sol. Cells*, 2020, **215**, 110606.
17 J. You, F. Guo, S. Qiu, W. He, C. Wang, X. Liu, W. Xu and Y. Mai, *J. Energy Chem.*, 2019, **38**, 192–198.
18 M. M. Lee, J. Teuscher, T. Miyasaka, T. N. Murakami and H. J. Snaith, *Science*, 2012, **338**, 643–647.
19 D. Di Girolamo, F. Matteocci, F. U. Kosasih, G. Chistiakova, W. Zuo, G. Divitini, L. Korte, C. Ducati, A. Di Carlo, D. Dini and A. Abate, *Adv. Energy Mater.*, 2019, **9**, 1901642.
20 R. A. Kerner and B. P. Rand, *J. Phys. Chem. Lett.*, 2017, **8**, 2298–2303.
21 S. Thampy, B. Zhang, K.-H. Hong, K. Cho and J. W. P. Hsu, *ACS Energy Lett.*, 2020, **5**, 1147–1152.
22 I. S. Zhidkov, D. W. Boukhvalov, A. I. Kukharenko, L. D. Finkelstein, S. O. Cholakh, A. F. Akbulatov, E. J. Juárez-Pérez, P. A. Troshin and E. Z. Kurmaev, *J. Phys. Chem. C*, 2020, **124**, 14928–14934.
23 M. Chen, Q. Dong, C. Xiao, X. Zheng, Z. Dai, Y. Shi, J. M. Luther and N. P. Padture, *ACS Energy Lett.*, 2022, 2256–2264.
24 D. Di Girolamo, E. Blundo, G. Folpini, C. Ponti, G. Li, M. H. Aldamasy, Z. Iqbal, J. Pascual, G. Nasti, M. Li, R. Avolio, O. Russina, A. Latini, F. Alharthi, M. Felici, A. Petrozza, A. Polimeni and A. Abate, *Phys. Status Solidi RRL*, 2021, **2100825**, 2100825.
25 S. Kahmann, S. Shao and M. A. Loi, *Adv. Funct. Mater.*, 2019, **29**, 1902963.
26 H.-H. Fang, S. Adjokatse, S. Shao, J. Even and M. A. Loi, *Nat. Commun.*, 2018, **9**, 243.
27 D. Di Girolamo, F. Di Giacomo, F. Matteocci, A. G. Marrani, D. Dini and A. Abate, *Chem. Sci.*, 2020, **11**, 7746–7759.
28 A. K. Baranwal, S. Saini, Y. Sanehira, G. Kapil, M. A. Kamarudin, C. Ding, S. R. Sahamir, T. Yabuki, S. Iikubo, Q. Shen, K. Miyazaki and S. Hayase, *ACS Appl. Energy Mater.*, 2022, **5**, 9750–9758.
29 T. Salim, S. Sun, Y. Abe, A. Krishna, A. C. Grimsdale and Y. M. Lam, *J. Mater. Chem. A*, 2015, **3**, 8943–8969.
30 M. Kot, L. Kegelmann, C. Das, P. Kus, N. Tsud, I. Matolinova, S. Albrecht, V. Matolin and D. Schmeisser, *ChemSusChem*, 2018, **11**, 3640–3648.
31 J. Dagar, S. Castro-Hermosa, G. Lucarelli, F. Cacialli and T. M. Brown, *Nano Energy*, 2018, **49**, 290–299.
32 J. Peng, J. I. Khan, W. Liu, E. Ugur, T. Duong, Y. Wu, H. Shen, K. Wang, H. Dang, E. Aydin, X. Yang, Y. Wan, K. J. Weber, K. R. Catchpole, F. Laquai, S. Wolf and T. P. White, *Adv. Energy Mater.*, 2018, **8**, 1801208.
33 J. Pascual, D. Di Girolamo, M. A. Flatken, M. H. Aldamasy, G. Li, M. Li and A. Abate, *Chem. – Eur. J.*, 2022, **28**(12), e202103919.
34 S. Gupta, D. Cahen and G. Hodes, *J. Phys. Chem. C*, 2018, **122**, 13926–13936.
35 J. Pascual, M. Flatken, R. Félix, G. Li, S. Turren-Cruz, M. H. Aldamasy, C. Hartmann, M. Li, D. Di Girolamo, G. Nasti, E. Hüsam, R. G. Wilks, A. Dallmann, M. Bär, A. Hoell and A. Abate, *Angew. Chem., Int. Ed.*, 2021, **60**, 21583–21591.
36 E. Jokar, C.-H. Chien, A. Fathi, M. Rameez, Y.-H. Chang and E. W.-G. Diau, *Energy Environ. Sci.*, 2018, **11**, 2353–2362.
37 X. Liu, Y. Wang, T. Wu, X. He, X. Meng, J. Barbaud, H. Chen, H. Segawa, X. Yang and L. Han, *Nat. Commun.*, 2020, **11**, 1–7.
38 E. Jokar, C. H. Chien, C. M. Tsai, A. Fathi and E. W. G. Diau, *Adv. Mater.*, 2019, **31**, 1–7.